ARTICLE
Journal of Cellular Biochemistry 113:824–832 (2012)

Journal of Cellular Biochemistry

Simultaneous Contraction and Buckling of Stress Fibers in Individual Cells

Shinji Deguchi,[1*] Tsubasa S. Matsui,[1] and Masaaki Sato[1,2]

[1]*Department of Biomedical Engineering, Tohoku University, Sendai, Japan*

[2]*Department of Bioengineering and Robotics, Tohoku University, Sendai, Japan*

ABSTRACT

It has been proposed that buckling of actin stress fibers (SFs) may be associated with their disassembly. However, much of the detail remains unknown partly because the use of an elastic membrane sheet, conventionally necessary for inducing SF buckling with a mechanical compression to adherent cells, may limit high quality and quick imaging of the dynamic cellular events. Here, we present an alternate approach to induce buckling behavior of SFs on a readily observable glass plate. Actin SFs were extracted from cells, and constituent myosin II (MII) molecules were partially photo-inactivated in contractility. An addition of Mg-ATP allowed actin–myosin cross-bridge cycling and resultant contraction of only thick SFs that still contained active MII in the large volume. Meanwhile, thin SFs with virtually no active motor protein in the small volume had no choice but to buckle with the shortening movement of nearby thick SFs functioning as a compression-inducing element. This novel technique, thus allowing for selective inductions of contraction and buckling of SFs and measurements of the cellular prestress, may be applicable to not only investigations on their disassembly mechanisms but also to measurements of the relative thickness of individual SFs in each cell. J. Cell. Biochem. 113: 824–832, 2012.

KEY WORDS: MECHANOBIOLOGY; STRESS FIBER; NON-MUSCLE MYOSIN II; ACTIN CYTOSKELETON; MECHANICAL STRESS

It has increasingly become clear that myosin-based contractility plays essential roles in cell functions such as proliferation and differentiation [Engler et al., 2006]. The cellular contractility is generated by cross-bridge cycling between non-muscle or smooth muscle myosin II (MII) and actin, which is also responsible for assembly of actin stress fibers (SFs) [Chrzanowska-Wodnicka and Burridge, 1996; Katoh et al., 2001a]. The tensional force produced in SFs is borne at the substrate via focal adhesions (FAs). Consequently, SFs in cells are under a condition of isometric contraction at which the macroscopic length along an SF from its one peripheral adhesion to another remains apparently unchanged while applying a physical force onto FAs [Peterson et al., 2004; Deguchi and Sato, 2009; Matsui et al., 2009].

SFs generating a tensional force are typically observed to have a tensed straight shape. Such straight SFs buckle to show a wavy pattern when the adherent cells are subject to a rapid mechanical compression [Costa et al., 2002; Lu et al., 2008]. It was reported that the appearance of buckling or tension release of SFs might be associated with their disassembly caused by mechanical stress to cells and resultant reorganization of cell structure [Sato et al., 2005; Matsui et al., 2011]. However, it is poorly understood how the buckling or tension release is related to the functions and structures of SFs.

In this article, we present a novel technique to simultaneously induce contraction and buckling of SFs, which may be useful in investigations on their mutual relationships and functions. Buckling behavior of SFs was conventionally produced by a tension release or mechanical compression of an elastic membrane sheet onto which cells are originally seeded [Costa et al., 2002; Sato et al., 2005; Lu et al., 2008]. Here, we describe an alternate method in which some SFs of individual cells are partially inactivated in contractility, followed by a contractility stimulation to remaining active SFs. Active SFs shorten in the entire length after the stimulation, whereas inactivated SFs are not able to contract and consequently exhibit buckling.

Additional supporting information may be found in the online version of this article.

Grant sponsor: Ministry of Education, Culture, Sports, Science, and Technology of Japan; Grant numbers: 21680039, 22650098, 20001007; Grant sponsor: Japan Society for the Promotion of Science; Grant number: 23-7552.

Shinji Deguchi's present address is Department of Bioengineering and Robotics, Tohoku University.

Tsubasa S. Matsui's present address is Department of Biomolecular Sciences, Tohoku University.

*Correspondence to: Shinji Deguchi, Ph.D., Department of Biomedical Engineering, Tohoku University, 6-6-01 Aramaki-Aoba, Sendai 980-8579, Japan. E-mail: deguchi@bml.mech.tohoku.ac.jp

Received 19 August 2011; Accepted 6 October 2011 • DOI 10.1002/jcb.23410 • © 2011 Wiley Periodicals, Inc.
Published online 20 October 2011 in Wiley Online Library (wileyonlinelibrary.com).

MATERIALS AND METHODS

CELL CULTURE

A7r5 vascular smooth muscle cells (ATCC, CRL-1444) were cultured in DMEM (Invitrogen) supplemented with 10% FBS (JRH Biosciences) and 1% penicillin–streptomycin (Invitrogen) at 37°C in 5% CO_2. Cells were cultured on an 18-mm square cover glass immersed in a plastic culture dish. Alternatively, cells were cultured in an elastic chamber with a 20-mm square transparent silicone (polydimethylsiloxane, PDMS) membrane at the bottom. The PDMS chamber was coated with 50 μg/ml fibronectin before cell seeding.

SOLUTIONS

Low ionic strength solution contained 2.5 mM triethanolamine, 1 mM DTT, 1 μg/ml leupeptin, and 1 μg/ml pepstatin. Wash solution contained 2 mM free Mg^{2+}, 20 mM imidazole, 2 mM EGTA, 10 mM DTT, 1 μg/ml leupeptin, and 1 μg/ml pepstatin. Activation solution contained 2 mM free Mg^{2+}, 20 mM imidazole, 2.1 mM $CaCl_2$, 2 mM EGTA, and 2.7 mM Mg-ATP. The pH was adjusted to 8.2 (low ionic strength solution) or 7.2 (wash and activation solutions) with KOH at room temperature (25°C). The total ionic strengths of wash and activation solutions were adjusted to 170 and 157 mM, respectively, with KCl.

CELL COMPRESSION

One end of the PDMS chamber was firmly attached to a fixed frame, while the other end was held on a movable frame. Cells were seeded onto the PDMS membrane and cultured for 2–3 days at 37°C in a CO_2 incubator. The PDMS membrane was uniformly stretched 40% in an axial direction and incubated for 2 h in the incubator. Cells were treated with 10 μM Y-27632 (Rho-kinase inhibitor, Wako) for 20 or 40 min. The membrane prestretch was then rapidly released to zero within 0.5 s by unhooking the mechanical connection between the frames. The release of the membrane prestretch resulted in a compression of the adhering cells. Cells were fixed soon after the compression with 4% paraformaldehyde for 10 min, washed with PBS, permeabilized with 0.1% Triton X-100 for 3 min, and stained with Alexa 488 phalloidin (Molecular Probes). Epifluorescence images were acquired on a microscope (IX-71, Olympus) using a CCD camera (ORCA-R2, Hamamatsu).

IMMUNOBLOTTING

Cells were treated with 10 μM Y-27632 for 20 min or 40 min or solvent vehicle (DMSO) for 40 min. Samples were solubilized in SDS-sample buffer, boiled for 5 min, fractionated on 12.5% polyacrylamide gels, and transferred onto polyvinylidene difluoride membranes (Millipore). Membranes were incubated with antibody against β-actin (1:1000, Applied Biological Materials), myosin light chain (MLC) (1:1000, Cell Signaling Technology), 1P-MLC (1:1000, Cell Signaling Technology), and 2P-MLC (1:1000, Cell Signaling Technology). The primary antibodies were detected using HRP-conjugated goat anti-mouse and goat anti-rabbit secondary antibodies (Bio-Rad Laboratories) and enhanced chemiluminescence (Immobilon Western, Millipore).

SF STIMULATION

Ventral SFs were extracted from cells according to the method described elsewhere [Matsui et al., 2010, 2011]. Briefly, cells cultured on the cover glass were washed twice with cold PBS. Cells were rinsed once with ice-cold low ionic strength solution, and de-roofed by exposing to repeated applications of fresh low ionic strength solution from a pipette. We confirmed using a phase-contrast microscope that the apical plasma membrane and most cellular organelles were removed, while ventral SFs remained on the cover glass. Low ionic strength solution was replaced with ice-cold wash solution. The cover glass supporting these extracted SFs was placed upside down over a glass plate to make a perfusion chamber using two parallel strips of scotch tape and a nail polish adhesive. The channel between the two glass surfaces was filled with wash solution with 3 nM Alexa 488 phalloidin for 1 min, and perfused with fresh wash solution from one side of the chamber via capillary action. The chamber was mounted on the microscope stage. The SFs were illuminated by a mercury lamp through an excitation filter (475–495 nm, Semrock) for ~30 s at a time. Activation solution was then perfused, and time-lapse epifluorescence images of SFs were captured using the CCD camera with an exposure time of 0.7 msec. Experiments were performed at room temperature. Fluorescence intensity measured along the length or across the width of SFs in acquired images was obtained by ImageJ (NIH).

IMMUNOSTAINING

Cells were fixed with 4% paraformaldehyde for 10 min, washed with PBS containing 30 mM glycine, permeabilized with 0.1% Triton X-100 for 3 min, treated with 10% normal goat serum in block ace for 1 h at room temperature. The cells were incubated with non-muscle MIIA (Covance) or IIB (Abcam) heavy chain mouse monoclonal antibody or diphosphorylated MLC rabbit polyclonal antibody (Cell Signaling) at 4°C overnight, incubated with the appropriate fluorescently-labeled secondary antibody, and then double-stained with Alexa phalloidin (Molecular Probes). Epifluorescence images were captured using ORCA-R2 camera.

RESULTS

COMPRESSION-INDUCED BUCKLING OF SFs

SFs were originally observed as straight actin bundles detected by fluorescent phalloidin (Fig. 1A). Buckling of SFs was observed when the PDMS chamber supporting cells was rapidly compressed. The buckling was observed over the cytoplasm even in cells treated with 10 μM Y-27632 for 20 min followed by the compression (Fig. 1B). In contrast, profound buckling was not observed in cells treated with Y-27632 for 40 min followed by the compression (Fig. 1C). Apparently, the thickness of SFs decreased in the cells treated with Y-27632 for 40 min compared to control cells. Changes in monophosphorylation of MLC at Ser19 (1P-MLC) and diphosphorylation of MLC at Thr18 and Ser19 (2P-MLC) were assessed by immunoblotting for cells treated with 10 μM Y-27632 for 20 min and 40 min (Fig. 1D). The relative amounts of 1P-MLC and 2P-MLC to total MLC showed that the MLC phosphorylations were significantly decreased in the cells treated with the Rho-kinase inhibitor compared with vehicle control (Fig. 1E).

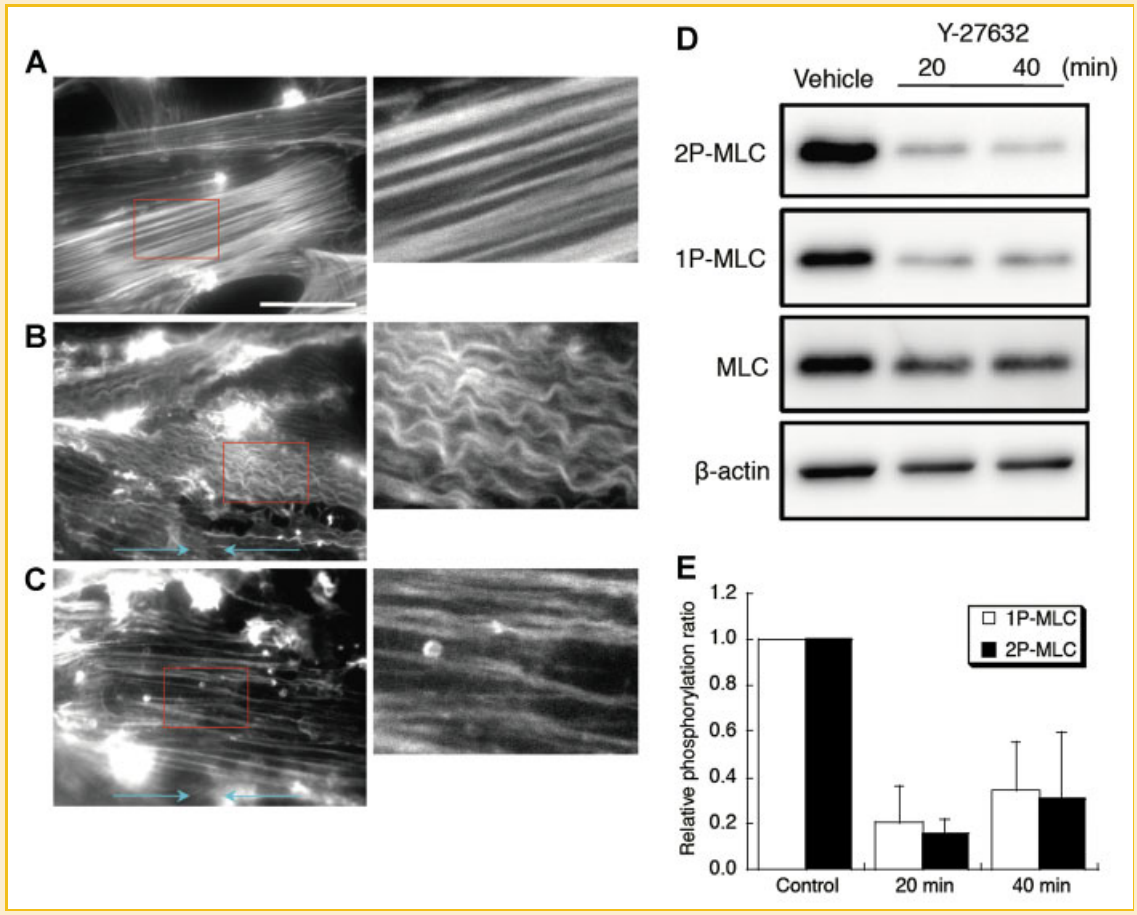

Fig. 1. Buckling of SFs. A: Actin filaments in control cells seeded on a PDMS membrane sheet. SFs were observed as straight actin bundles as shown in the enlarged image of the boxed area. B: Buckling of SFs appeared after 40% compression for cells treated with 10 μM Y-27632 for 20 min. C: Buckling of SFs was largely attenuated in cells treated with 10 μM Y-27632 for 40 min. D: Immunoblotting of cells treated with 10 μM Y-27632 showed that MLC phosphorylations were significantly decreased. Results are representative of three independent experiments. E: Corresponding analysis of MLC phosphorylations expressed relative to the MLC levels and normalized to the control (mean ± SD). The arrows on images represent the direction of compression. Scale bar, 20 μm. [Color figure can be seen in the online version of this article, available at http://wileyonlinelibrary.com/journal/jcb]

SIMULTANEOUS CONTRACTION AND BUCKLING OF SFs

SFs were extracted from cells and illuminated by a mercury lamp through a 475–495-nm filter for ~30 s. The extracted SFs containing actin-MII complexes in the rigor state were then reactivated with addition of 2.7 mM Mg-ATP. The whole cells slowly shrank in the axial direction taking more than 45 min. Among the extracted SFs, only apparently thick fibers shrank while keeping their straight shapes; meanwhile, thinner ones exhibited profound buckling behavior particularly at local places where the contraction of the thick SFs occurred (Fig. 2; see also supplementary online material video 1). It was confirmed by intensity profile examined in a direction perpendicular to SFs that the SFs that exhibited buckling had lower intensity than others that kept straight shapes without showing buckling (Fig. 3). We also separately confirmed that other extracted SFs in the cells placed in the same cover glass but outside the field of view fully contracted and collapsed into a tight mass no later than 45 min when we ceased the observations of SFs of original interest.

PRESTRAIN IN SFs

All SFs extracted from cells slowly shrank upon the addition of Mg-ATP, but while thick fibers continued to shorten over time other thin fibers eventually exhibited buckling (Figs. 2 and 3). Such thin SFs started to buckle when their axial length decreased to 87 ± 6.5% of the original length (Fig. 4; mean ± SD, n = 14 SFs). Assuming that the buckling occurred when the SFs reached their zero-stress length, prestrain in the SFs was obtained as the displacement (the original length minus the zero-stress length) divided by the zero-stress length to be on an average 0.15 (Fig. 4).

MYOSIN DISTRIBUTIONS

Intracellular distributions of MIIs were assessed using an antibody against MIIA and IIB. MIIA and MIIB were observed along the length of both apparently thick and thin actin bundles detected by fluorescent phalloidin binding (Fig. 5). F-actin had relatively uniform staining pattern, whereas MIIs were observed as a dotted sarcomeric pattern. The presence of diphosphorylated MLC in both

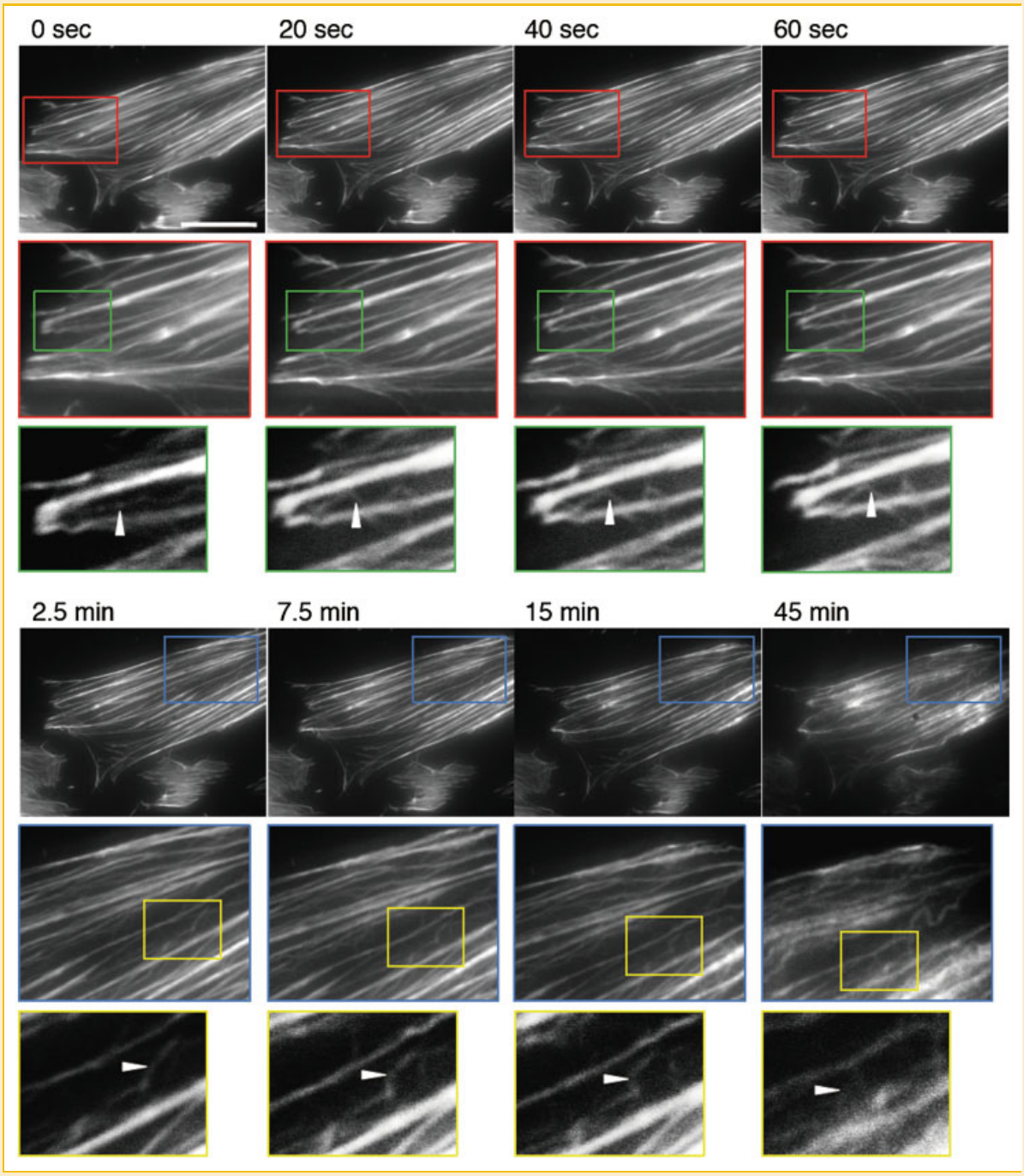

Fig. 2. Simultaneous contraction and buckling of SFs. Extracted SFs were pre-illuminated by a mercury lamp and then stimulated with Mg-ATP. Some SFs responded to Mg-ATP to contract, while other fibers (indicated by arrowheads in the higher-magnification images of the boxed areas) exhibited buckling as the whole cell shortened. See also supplementary online material video 1. Scale bar, 20 μm. [Color figure can be seen in the online version of this article, available at http://wileyonlinelibrary.com/journal/jcb]

SFs in intact cells (Fig. 6A) and extracted SFs (Fig. 6B) was observed as a dotted sarcomeric pattern regardless of their apparent thickness.

DISCUSSION

In this article, we demonstrated that simultaneous contraction and buckling of SFs occurred in individual cells after a partial inactivation of MIIs followed by administration of Mg-ATP. A conventional technique for inducing SF buckling uses elastic membrane sheets onto which cells to be compressed are seeded. This common technique is useful in controlling the magnitude of the compression and resultant buckling of all SFs aligned in the compression direction. However, the use of such membranes may be unsuitable for high quality and/or quick imaging of the buckling

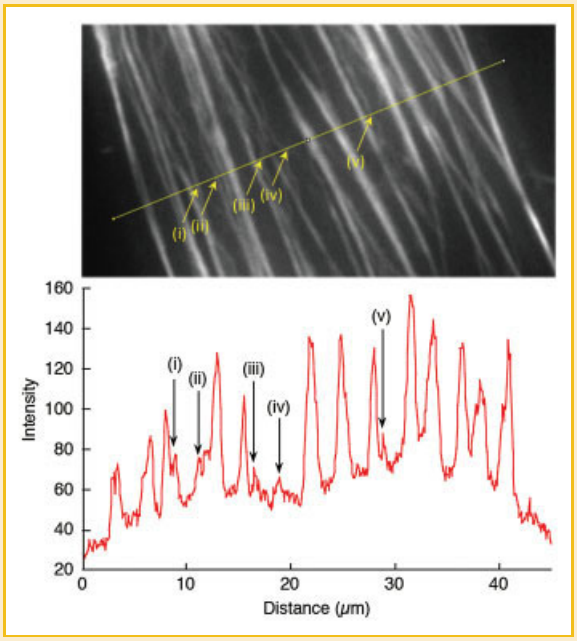

Fig. 3. Evaluation of SF thickness. The profile scan along the indicated line drawn perpendicular to the major axis of the cell shows that SFs that exhibited buckling (i–v in the inset image taken from "15 min" of Fig. 2) have low F-actin intensity and hence are thin in width. [Color figure can be seen in the online version of this article, available at http://wileyonlinelibrary.com/journal/jcb]

behavior and dynamic cellular events following the buckling. On the other hand, by applying the novel technique presented here, selective buckling and contraction of SFs in individual cells could be induced on a readily observable glass plate.

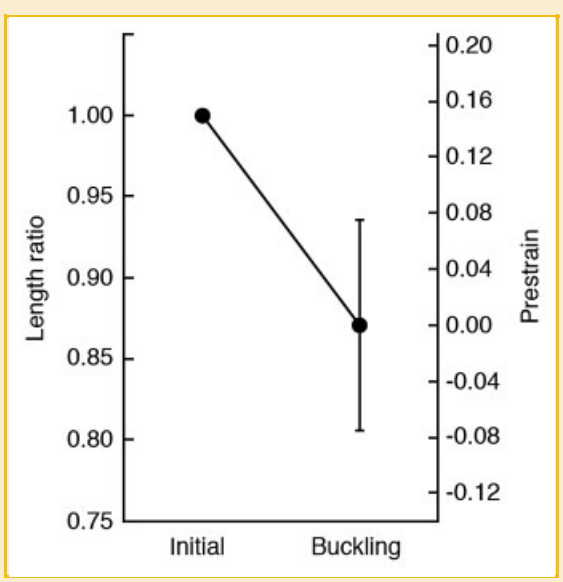

Fig. 4. Change in SF length just before reaching buckling. Prestrain was calculated from the mean value as the ratio of the initial length (before stimulation with Mg-ATP) to the non-stress length.

Our group previously demonstrated that SFs labeled with fluorescent phalloidin are able to contract by administrating 2.7 mM Mg-ATP contained in a solution with the ionic strength of 157 mM [Matsui et al., 2011]. The previous method for inducing the complete SF contraction is essentially the same as that used in the present study using the same Mg-ATP concentration and ionic strength, but differs in two respects. Firstly, the previous study used oxygen-removal reagents consisting of glucose, catalase, and glucose oxidase. With these chemicals, we confirmed in separate experiments that long-term observations of SF contraction for more than 2 h were possible (figure not shown). Another major difference between the previous and present methods was the use of a brief pre-illumination. We were aware that fluorescently labeled SFs did not often exhibit contraction when they were illuminated using a mercury lamp prior to observations for a relatively long time of 1 min at a time. In the present study, we illuminated fluorescent SFs extracted from cells for nearly 30 s at a time, shorter than that resulted in complete inhibition of SF contraction. With addition of Mg-ATP to the pre-illuminated samples, some SFs gradually contracted as other ones buckled (Fig. 2). Intensity measurement shows that the SFs that exhibited buckling were lower in F-actin intensity than the other ones that contracted with straight shapes (Fig. 3), indicating that thick SFs contracted as relatively thin SFs buckled.

MIIs and phosphorylated MLC responsible for Mg-ATP-induced contraction were observed over the cytoplasm, not only in thick SFs but also in thin SFs (Figs. 5 and 6). It is likely that the brief pre-illumination without oxygen-removal reagents partially inactivates the motor activity of the MIIs in the thick as well as thin SFs. SFs are known to have a variety of thickness, ranging from 100 to 500 nm in endothelial cells and smooth muscle cells [Deguchi et al., 2005a, 2006]. Assuming that the number of MIIs contained in SFs is proportional to the bundle size, we speculate that the partial photo-inactivation of MIIs is critical for the contractile ability of thin SFs having a limited number of MIIs in the lateral direction (Fig. 7). The thin SFs in which a majority of MIIs are photo-inactivated are no longer able to respond to Mg-ATP for contractile activity. In contrast, relatively thick SFs, originally having greater numbers of MIIs in the large volume, could still contain active MIIs in their lateral direction even after the pre-illumination. Such survived MIIs, even if limited in number compared to the original condition, are enough to pull on nearby actin filaments and consequently shorten the macroscopic length of the SFs. The thin SFs, being unable to shrink, have no choice but to buckle in such conditions because there would be some physical cross-links or internal friction between the thin SFs and thick SFs through direct or indirect connections via cortical layers or actin meshwork [Deguchi et al., 2005b; Russell et al., 2009], which should function as a compression-induced element (Fig. 7).

The model illustrated in Figure 7 is in agreement with the macroscopic rate of the contraction we observed. Specifically, it took 60 s for the pre-illuminated SFs to shorten ~10 μm after the addition of Mg-ATP (Fig. 2). The shortening rate is therefore estimated to be roughly <0.2 μm/sec, which is much lower compared to our previous observation that fluorescent SFs contracted at 0.8 μm/sec at the same Mg-ATP concentration [Matsui

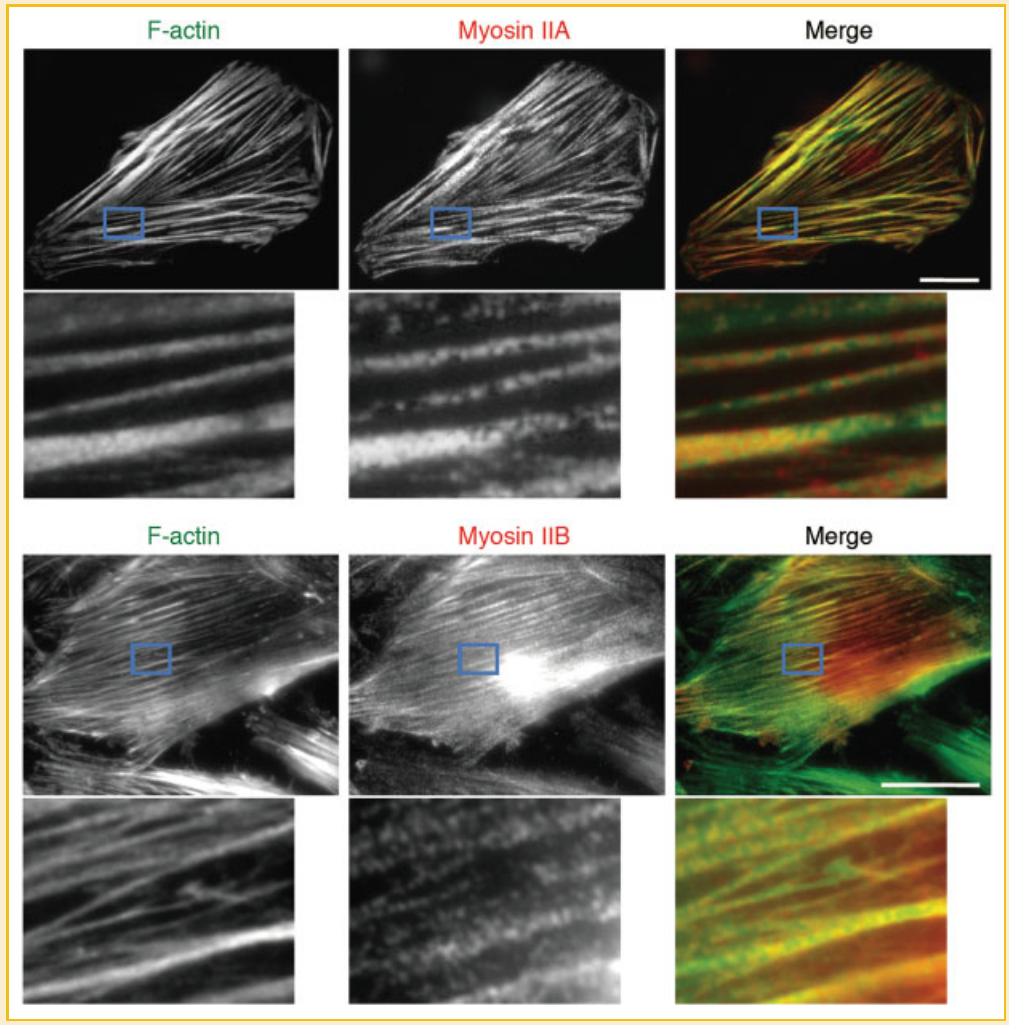

Fig. 5. Colocalizations of MIIA and MIIB with actin bundles. Higher-magnification images of the boxed areas are also shown. Scale bars, 20 μm. [Color figure can be seen in the online version of this article, available at http://wileyonlinelibrary.com/journal/jcb]

et al., 2011]. Thus, probably because of the decreased number of active MIIs after the photo-inactivation, a slower contraction compared to more intact conditions was observed. This is also consistent with our observation that other SFs located outside the field of view and hence unexposed to the illumination were able to fully contract to collapse into a tight mass in response to Mg-ATP.

Given that the selectivity of buckling and contraction thus depends on the thickness of the SFs, this technique could be developed for estimating the thickness of individual SFs in living cells without using electron microscopy. The thickness measurement may be useful for analysis of spatial regulations of SFs in individual cells. It has been proposed that distinct pathways for MLC phosphorylation, responsible for MII activation and resulting assembly of SFs, are spatially regulated [Katoh et al., 2001a, 2001b; Tanner et al., 2010]. Specifically, Rho-kinase and myosin light chain kinase have been implicated as a predominant kinase for the MLC phosphorylations at the central and peripheral parts of the cells, respectively. Although the mechanisms of the specific and differential contributions of each kinase remain understood, Katoh et al. [2001b] showed using electron microscopy that peripheral SFs were thicker than central SFs in fibroblasts and implicated that the structural difference might be related to the spatial regulation mechanisms. We did not find in the present observations on A7r5 smooth muscle cell lines that central SFs are entirely thinner than peripheral SFs and hence are prone to buckle. Rather, thin (buckled) and thick (non-buckled) SFs were alternately found in the cytoplasm (Figs. 2 and 3), from which we suspect that the spatial regulation based on either Rho-kinase or myosin light chain kinase might be a cell type-specific phenomenon. Experiments using the present technique with more localized inactivation of MIIs by a laser illumination might be useful to more definitively characterize distinct roles of thick and thin SFs in a variety of cells.

Another possible application of the present technique is a measurement of the prestress (or prestrain) in adherent cells. We demonstrated that the prestrain in SFs estimated from a length change necessary for causing buckling was on an average 0.15 (Fig. 4). Interestingly, this value is comparable in magnitude to the prestrain obtained in Lu et al. [2008], 0.10 for human aortic

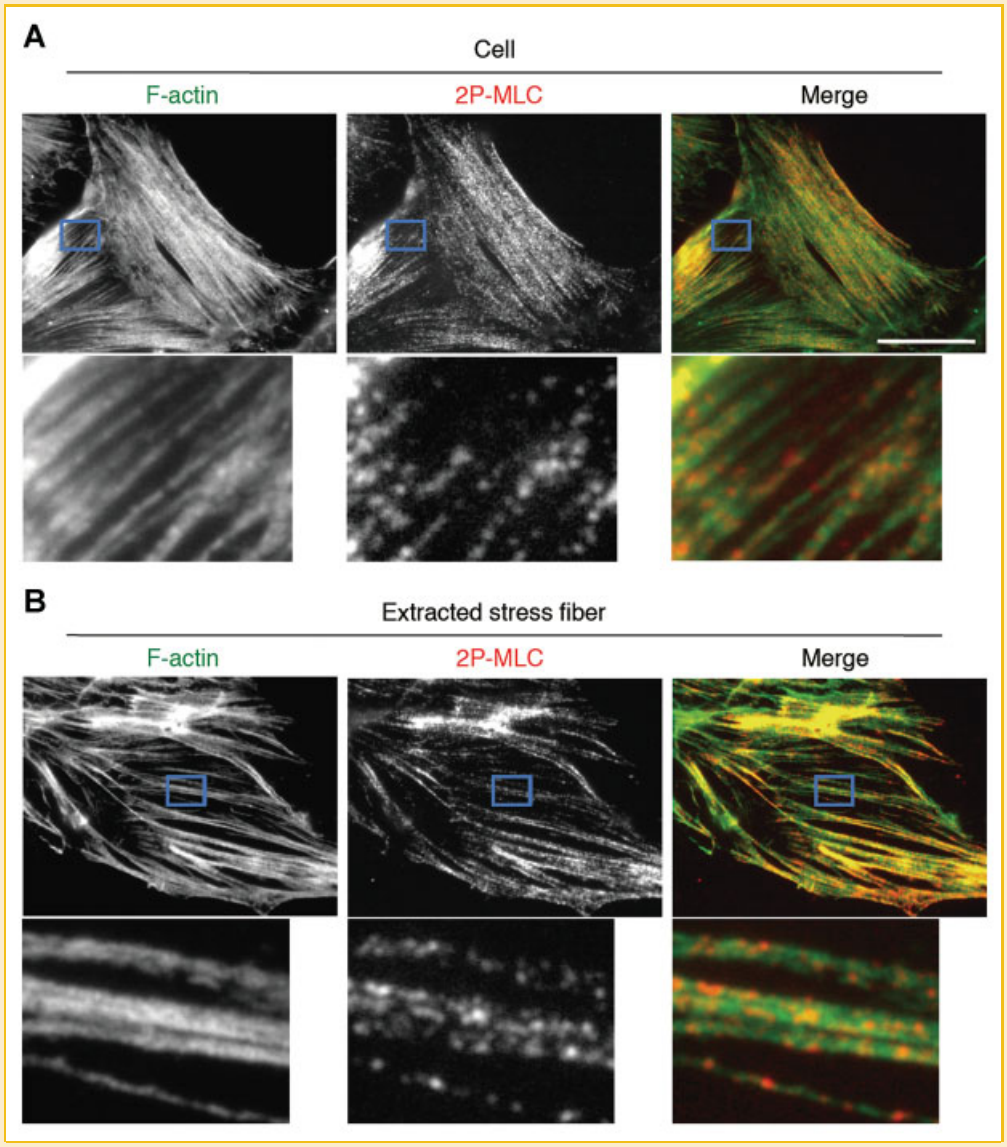

Fig. 6. Colocalizations of diphosphorylated MLC with actin bundles. A: SFs in intact cells. B: SFs extracted from cells. Higher-magnification images of the boxed areas are also shown. Scale bar, 20 μm. [Color figure can be seen in the online version of this article, available at http://wileyonlinelibrary.com/journal/jcb]

endothelial cells, in which a length change leading to buckling after compression of cells on a membrane sheet was measured. It is likely that the cell prestrain is generated due to the contractile activity of ubiquitous MIIs, resulting in that the intracellular stress-bearing components are physically extended beyond their unloaded length [Stamenović and Ingber, 2002; Wang et al., 2002; Paul et al., 2008; Park et al., 2010; Kaunas et al., 2011]. Quantification of prestrain magnitude and its spatial distribution in individual cells is important for accurate understanding of intracellular force transmission triggering mechanical stress-elicited functions. Of particular interest is the relationship between the prestrain magnitude and MLC phosphorylation. Profound buckling of SFs was observed in cells treated with Y-27632 for 20 min (Fig. 1B), which led to a decrease in MLC phosphorylation (Fig. 1E). In contrast, a further treatment with Y-27632 for 40 min caused extensive disassembly or unbundling of SFs [Matsui et al., 2010] and significantly attenuated their buckling (Fig. 1C). We speculate that the prolonged treatment with Y-27632 significantly reduces the cellular contractility and hence dissipates the prestrain. Therefore, axial compressive forces yielding the buckling may not properly be transmitted within such relaxed SFs. The present technique enabling selective buckling, without using a membrane sheet that limits high quality and quick imaging of dynamic cellular events, may contribute to revealing the mechanisms underlying these phenomena.

In conclusion, we presented a novel technique to induce contraction and buckling of SFs simultaneously in individual cells. A brief pre-illumination to cells resulted in partial inactivation of the motor activity of MIIs inside SFs. Thin SFs with virtually no active MII across their widths are not able to respond to Mg-ATP for contraction, whereas relatively thick SFs that still contain active

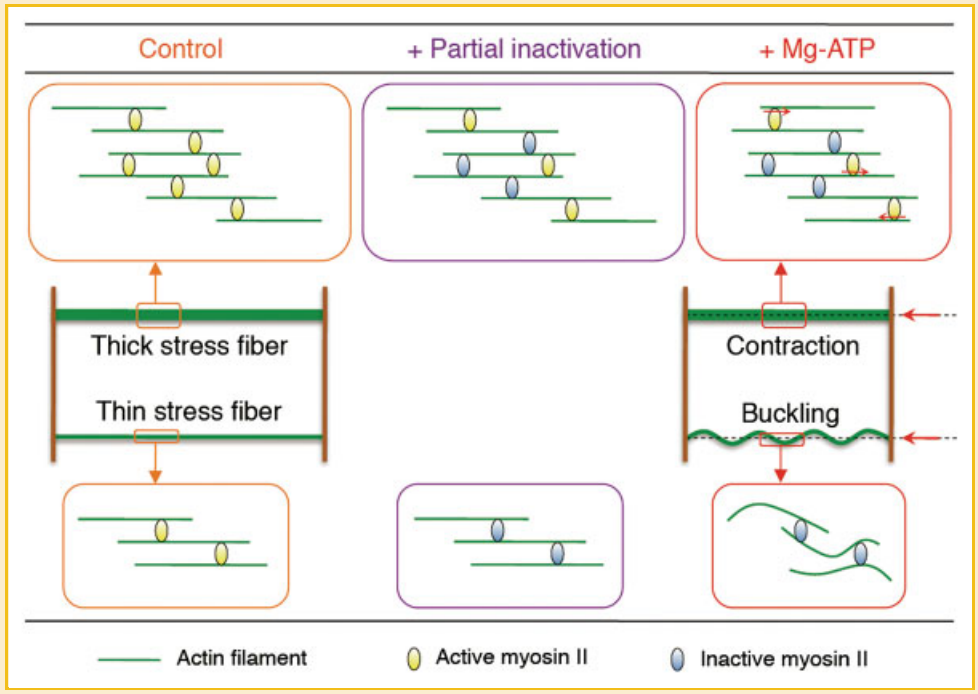

Fig. 7. A schematic interpretation of the simultaneous contraction of thick SFs and buckling of thin SFs. With a brief pre-illumination, virtually all MIIs are inactivated in thin SFs, while some MIIs in thick SFs are still active to move along the constituent actin filaments. These survived MIIs may be enough to contract the whole actin bundles in response to an addition of Mg-ATP. The shortening movements of the thick SFs compress nearby thin SFs, being unable to contract by themselves, to finally induce buckling of the non-contractile thin SFs. [Color figure can be seen in the online version of this article, available at http://wileyonlinelibrary.com/journal/jcb]

MIIs shrink at a slow rate. Such thin SFs have no choice but to buckle with a shortening movement of nearby thick SFs functioning as a compressing element. This technique, thus allowing for selective inductions of contraction and buckling, may be applicable to measurement of the relative thickness of individual SFs in cells and evaluation of their functions in terms of thickness. In addition, the new technique for generating buckling of SFs without a use of an elastic membrane sheet, which is unsuitable for high quality and/or quick imaging, may be useful in investigations on their disassembly mechanisms that have been proposed to be associated with their buckling.

ACKNOWLEDGMENTS

The authors thank Hitomi Onodera for technical assistance. This work was supported by Special Coordination Funds for Promoting Science and Technology (to S.D.), and in part by Grants-in-Aid from the Ministry of Education, Culture, Sports, Science, and Technology of Japan (#21680039 and #22650098 to S.D. and #20001007 to M.S.) and by a Grant-in-Aid for JSPS Fellows (#23-7552 to T.S.M.) from Japan Society for the Promotion of Science.

REFERENCES

Chrzanowska-Wodnicka M, Burridge K. 1996. Rho-stimulated contractility drives the formation of stress fibers and focal adhesions. J Cell Biol 133: 1403–1415.

Costa K, Hucker WJ, Yin F. 2002. Buckling of actin stress fibers: A new wrinkle in the cytoskeletal tapestry. Cell Motil Cytoskeleton 52:266–274.

Deguchi S, Ohashi T, Sato M. 2005a. Evaluation of tension in actin bundle of endothelial cells based on preexisting strain and tensile properties measurements. Mol Cell Biomech 2:125–133.

Deguchi S, Ohashi T, Sato M. 2005b. Intracellular stress transmission through actin stress fiber network in adherent vascular cells. Mol Cell Biomech 2:205–216.

Deguchi S, Ohashi T, Sato M. 2006. Tensile properties of single stress fibers isolated from cultured vascular smooth muscle cells. J Biomech 39:2603–2610.

Deguchi S, Sato M. 2009. Biomechanical properties of actin stress fibers of non-motile cells. Biorheology 46:93–105.

Engler AJ, Sen S, Sweeney HL, Discher DE. 2006. Matrix elasticity directs stem cell lineage specification. Cell 126:677–689.

Katoh K, Kano Y, Amano M, Onishi H, Kaibuchi K, Fujiwara K. 2001a. Rho-kinase–mediated contraction of isolated stress fibers. J Cell Biol 153:569–584.

Katoh K, Kano Y, Amano M, Kaibuchi K, Fujiwara K. 2001b. Stress fiber organization regulated by MLCK and Rho-kinase in cultured human fibroblasts. Am J Physiol Cell Physiol 280:C1669–C1679.

Kaunas R, Hsu HJ, Deguchi S. 2011. Sarcomeric model of stretch-induced stress fiber reorganization. Cell Health Cytoskeleton 3:13–22.

Lu L, Feng Y, Hucker WJ, Oswald SJ, Longmore GD, Yin FC. 2008. Actin stress fiber pre-extension in human aortic endothelial cells. Cell Motil Cytoskeleton 65:281–294.

Matsui TS, Deguchi S, Sakamoto N, Ohashi T, Sato M. 2009. A versatile micro-mechanical tester for actin stress fibers isolated from cells. Biorheology 46:401–415.

Matsui TS, Ito K, Kaunas R, Sato M, Deguchi S. 2010. Actin stress fibers are at a tipping point between conventional shortening and rapid disassembly at physiological levels of MgATP. Biochem Biophys Res Commun 395:301–306.

Matsui TS, Kaunas R, Kanzaki M, Sato M, Deguchi S. 2011. Non-muscle myosin II induces disassembly of actin stress fibres independently of myosin light chain dephosphorylation. Interface Focus 1:754–766.

Park CY, Tambe D, Alencar AM, Trepat X, Zhou EH, Millet E, Butler JP, Fredberg JJ. 2010. Mapping the cytoskeletal prestress. Am J Physiol Cell Physiol 298:C1245–C1252.

Paul R, Heil P, Spatz JP, Schwarz US. 2008. Propagation of mechanical stress through the actin cytoskeleton toward focal adhesions: Model and experiment. Biophys J 94:1470–1482.

Peterson LJ, Rajfur Z, Maddox AS, Freel CD, Chen Y, Edlund M, Otey C, Burridge K. 2004. Simultaneous stretching and contraction of stress fibers in vivo. Mol Biol Cell 15:3497–3508.

Russell RJ, Xia SL, Dickinson RB, Lele TP. 2009. Sarcomere mechanics in capillary endothelial cells. Biophys J 97:1578–1585.

Sato K, Adachi T, Matsuo M, Tomita Y. 2005. Quantitative evaluation of threshold fiber strain that induces reorganization of cytoskeletal actin fiber structure in osteoblastic cells. J Biomech 38:1895–1901.

Stamenović D, Ingber DE. 2002. Models of cytoskeletal mechanics of adherent cells. Biomech Model Mechanobiol 1:95–108.

Tanner K, Boudreau A, Bissell MJ, Kumar S. 2010. Dissecting regional variations in stress fiber mechanics in living cells with laser nanosurgery. Biophys J 99:2775–2783.

Wang N, Tolić-Nørrelykke IM, Chen J, Mijailovich SM, Butler JP, Fredberg JJ, Stamenović D. 2002. Cell prestress. I. Stiffness and prestress are closely associa-ted in adherent contractile cells. Am J Physiol Cell Physiol 282:C606–C616.